Mean energy, energy-range relationships and depth-scaling factors for clinical electron beams

G. X. Ding,[a] and D. W. O. Rogers[b),c)]
Ionizing Radiation Standards, Institute for National Measurement Standards, National Research Council of Canada, Ottawa K1A 0R6, Canada

T. R. Mackie
Department of Medical Physics, University of Wisconsin, Madison, Wisconsin 53706

87.53.03
87.55.08.
87.53.10.j

(Received 14 April 1995; accepted for publication 29 August 1995)

Using Monte Carlo simulations we have studied the electron mean energy, $\bar{E}_o$, and the most probable energy, $E_{o,p}$, at the phantom surface and their relationships with half-value depth, R_{50}, and the practical range, R_p, for a variety of beams from five commercial medical accelerators with an energy range of 5–50 MeV. It is difficult to obtain a relation between R_{50} and $\bar{E}_o$ for all electrons at the surface because the number of scattered lower-energy electrons varies with the machine design. However, using only direct electrons to calculate $\bar{E}_o$, there is a relationship which is in close agreement with that calculated using monoenergetic beams by Rogers and Bielajew [Med. Phys. **13**, 687–694 (1986)]. We show that the empirical formula $E_{o,p}=0.22+1.98R_p+0.0025R_p^2$ describes accurately the relationship between R_p and $E_{o,p}$ for clinical beams of energies from 5 to 50 MeV with an accuracy of 3%. The electron mean energy, $\bar{E}_d$, is calculated as a function of depth in water as well as plastic phantoms and is compared both with the relation, $\bar{E}_d=\bar{E}_o(1-d/R_p)$, employed in AAPM protocols and with values in the IAEA Code of Practice. The conventional relations generally overestimate $\bar{E}_d$ over the entire therapeutic depth, e.g., the AAPM and IAEA overestimate $\bar{E}_d$ at d_{max} by up to 20% for an 18 MeV beam from a Clinac 2100C. It is also found that at all depths mean energies are 1%–3% higher near the field edges than at the central axis. We calculated depth-scaling factors for plastic phantoms by scaling the depth in plastics to the water-equivalent depth where the mean energies are equal. The depth-scaling factor is constant with depth in a given beam but there is a small variation ($<1.5\%$) depending on the incident beam energies. Depth-scaling factors as a function of R_{50} in plastic or water are presented for clear polystyrene, white polystyrene and PMMA phantom materials. The calculated depth-scaling factor is found to be equal to $R_{50}^{water}/R_{50}^{plastic}$. This is just the AAPM definition of effective density but there are up to 2% discrepancies between our calculated values and those recommended by the AAPM and the IAEA protocols. We find that the depth-scaling factors obtained by using the ratio of continuous-slowing-down ranges are inaccurate and overestimate our calculated values by 1%–2% in all cases. We also find that for accurate work, it is incorrect to use a simple $1/r^2$ correction to convert from parallel beam depth-dose curves to point source depth-dose curves, especially for high-energy beams.

Key words: mean electron energy, clinical electron beams, energy-range relations, depth-scaling factor, Monte Carlo

I. INTRODUCTION

The dose distributions produced by an electron beam depend strongly upon the beam's energy distribution and other aspects of the beam's quality. Clinical electron beams can be characterized by a number of parameters. The mean energy and the most probable energy of electrons at a phantom surface are two important parameters for electron beams as they are used for the choice of energy dependent dosimetric parameters, such as the stopping-power ratios and the electron fluence correction factors.

A. Most probable and mean energies on the surface

The most probable energy of the electron beam at the surface of the phantom, $E_{o,p}$, is related to the practical range in water, R_p (in cm), by the relationship[1–4]

$$E_{o,p}=0.22+1.98R_p+0.0025R_p^2 \quad \text{(MeV)}. \tag{1}$$

Equation (1) was first obtained by fitting the experimental results for nearly monoenergetic 10 to 50 MeV electron beams from a Racetrack microtron.[5] This is a modification of the linear Markus energy-range formula ($E_{o,p}=1.95R_p+0.48$).[6] From 1 to 50 MeV, Eq. (1) agrees within 1% with practical ranges extracted from Berger and Seltzer's Monte Carlo calculated depth-dose curves.[3,7] It has also been found that Eq. (1) reproduces the measured data with an accuracy of 2% from 5 to 50 MeV.[1,3] The Monte Carlo calculations[8] by Rogers and Bielajew have generated similar values except at high energies where EGS4 calculations predict energies which are 4% to 6% less than predicted by the ICRU/ETRAN results.[8] Sorcini and Brahme have used a general analytical energy-range relation to relate R_p to

$E_{o,p}$ of incident electron beams in the range 1 to 50 MeV for absorbers of any atomic number.[9] However, for water their results are very similar to those in Eq. (1).

Several dosimetry protocols[1,2,4,10] recommend the following relationship for the determination of the mean energy of the electron beam at the surface of the phantom:

$$\bar{E}_o = 2.33 R_{50} \quad (\text{MeV}), \tag{2}$$

where $\bar{E}_o$ is the mean energy and R_{50} is the depth in cm of either the 50% ionization or dose levels. The value of 2.33 MeV/cm was recommended by the AAPM TG-21 protocol[2] and was obtained from an analysis of depth–dose curves calculated by Berger and Seltzer[11] for plane-parallel, infinitely wide beams of monoenergetic electrons incident upon a semi-infinite water phantom. This value was an average for values in the energy range 5–50 MeV and, as pointed out by Wu *et al.*,[12] is applicable to the 50% value of the depth-dose curve although TG–21 applied it to depth-ionization curves. The same value of 2.33 MeV/cm was recommended by Brahme and Svensson[13] based on measurements for depth-dose curves corrected to infinite SSD although they also explicitly state that their results are in agreement with the Monte Carlo calculations of Berger and Seltzer. After isolating an error in the earlier Monte Carlo calculations with ETRAN, Rogers and Bielajew (RB–86)[8] used the EGS4 Monte Carlo system to calculate and to tabulate $\bar{E}_o$ as a function of R_{50} for various values of SSD. Their results systematically give higher $\bar{E}_o$ values and are recommended in the AAPM TG–25 Report[10] for more accurate estimates of the mean energy of electron beams.

The above relationships are based on depth–dose curves. The IAEA[4] and the NACP[1] protocols tabulate values which use the half–value depth measured from either absorbed dose or ionization curves at SSD=100 cm and we have recently presented explicit data to facilitate using either the depth of 50% dose or ionization.[14] In the remainder of this paper we deal exclusively with range parameters based on depth–dose curves.

In the previous studies mentioned above, either parallel, monoenergetic beams were used in Monte Carlo calculations or the "measurements" used approximate methods to estimate the energy of the beam. With the development of a Monte Carlo code to simulate realistic electron beams (described below), we can investigate the accuracy of these previous approximations. Udale-Smith has done a similar study previously[15] for 3 specific machines and found considerable disagreement with various energy-range relationships. However, as reported previously, there are some unexplained differences between her calculated spectra and ours, with mean energies on the surface differing by up to 300 keV for the 10 MeV beam from an SL75/20.[16]

B. Mean electron energy as a function of depth in a phantom

The mean electron energy as a function of depth in the phantom is needed for the choice of the replacement correction for absorbed dose measurements with an ion chamber. Harder's relation is employed in the AAPM protocol[2,10] to estimate the mean electron energy:

$$\bar{E}_d = \bar{E}_o(1 - d/R_p), \tag{3}$$

where $\bar{E}_o$ is the average incident electrons energy at the phantom surface, d is the depth of measurement and R_p is the practical range in the same units as the depth.

Instead of Harder's relationship, the IAEA recommends using the Monte Carlo results of Andreo and Brahme[17] for the evaluation of $\bar{E}_d$ given $\bar{E}_o$ and d/R_p. These calculations are for monoenergetic broad parallel incident beams. The mean electron energy is calculated for the primary electrons and the secondary electrons created in the phantom are not included. Since there are secondary electrons created in the phantom, it is interesting to see how this will affect the mean electron energy in phantoms.

As well as changes from considering secondary electrons in the phantom, clinical beams have energy and angular distributions which introduce uncertainty even if the mean energy of the clinical beams is estimated correctly and used with calculations for monoenergetic beams. Udale-Smith has calculated $\bar{E}_d$ values for all electrons and compared calculations with monoenergetic incident beams to those using simulated clinical beams from SL75 machines for beam energies less than 12 MeV.[15] Her results showed that the value of $\bar{E}_d$ for the monoenergetic beams decreased with depth more quickly than that of the simulated clinical beam.

C. Depth-scaling for plastic phantoms

It is recommended by major dosimetry protocols[2,10,4] that water be used as the standard phantom material for the dosimetry of high-energy electrons. However it is not always possible or practical to perform dosimetry measurements in a water phantom. In this case it is necessary to scale depths measured in non-water phantoms to water equivalent depths. One form of depth-scaling is range scaling whereby the range in one material is used to deduce the corresponding range in water. Using Monte Carlo methods, Grosswendt and Roos[18] calculated depth-dose curves in different phantom materials for monoenergetic broad electron beams with incident energies between 1 and 10 MeV. From these the corresponding values of R_{50} and R_p were deduced and compared to the predictions for a variety of protocols. Their results showed that deviations in the range scaling from different recommendations and in the energy-range relations for water may accumulate to give errors in assigned energies of several percent.

As an example of this type of range scaling, the IAEA recommends scaling R_p and R_{50} (in cm) to water equivalent ranges using:[4]

$$\frac{R_{plastic}}{R_{water}} = \frac{(r_o/\rho)_{plastic}}{(r_o/\rho)_{water}} \tag{4}$$

where r_o/ρ is the linear continuous-slowing-down range (in cm) tabulated as a function of energy by the ICRU.[3] The mean energy at the phantom surface is used as an input parameter for the choice of the ratios.

Depth scaling can also be done for other purposes. In the AAPM TG-21 and TG-25 protocols, the objective is to find depths at which the electron spectra are identical so that one can predict absolute dose in water given an ion chamber reading in plastic at the scaled depth. The spectra are assumed identical if the mean energies are the same. The AAPM TG-25 protocol[10] recommends that the water-equivalent depth be determined by scaling the depth in plastic by the ratio of R_{50} values, i.e.:

$$d_{water}=d_{med}\times\rho_{eff}=d_{med}\left(\frac{R_{50}^{water}}{R_{50}^{med}}\right)\ [\text{cm}], \tag{5}$$

where ρ_{eff} is the effective density for non-water phantoms. The recommended values of ρ_{eff} in the AAPM TG-25 protocol[10] are based exclusively on R_{50} measurements of an 18 MeV beam. The IAEA Code of Practice does depth-scaling in the same manner as described above for range-scaling.

D. The BEAM code

BEAM is a general-purpose Monte Carlo simulation code[16] which is based on the EGS4 Monte Carlo system.[19] BEAM allows the simulation of radiotherapy treatment units and produces data on realistic clinical beams. It has been extensively benchmarked against measured dose distributions for a variety of accelerators and excellent agreement was obtained in central-axis percentage depth-dose as well as in dose-profile curves.[16,20] The excellent agreement indicates that the simulated clinical beams are accurate. However, the energy of the assumed monoenergetic beam of electrons leaving the accelerator vacuum is a parameter which is adjusted to match the experimental value of R_{50}. In one case the incident electron energy was known independently with an accuracy of $\pm 1\%$ and the calculated values of R_{50} agreed with the experimental values within 1.5%. This suggests an established overall accuracy on the energies of only 1% to 2%. However, a major thrust of this work is to study the effects of using incident realistic vs monoenergetic beams so that even with an overall error of 2%, a difference of 0.2% is likely calculated accurately.

E. Outline

Using the simulated realistic clinical beams we calculate various beam parameters: $\bar{E}_o$, $E_{o,p}$, R_{50} and R_p. The two empirical formulae [Eqs. (1) and (2)] commonly used in electron beam dosimetry can be tested against simulated realistic clinical beams, in addition, $\bar{E}_d$ as a function of depth can be calculated using realistic clinical beams.

As mentioned above, the purpose of depth-scaling is to scale the depth measured in a non-water phantom to the water-equivalent depth in water where the electron energy spectra are identical. Because energy-loss straggling and multiple scattering depend upon the effective atomic number of the phantoms, it is difficult to find corresponding depths where the energy spectra are identical. However, there are corresponding depths where the mean energies are identical. The TG-25 protocol assumes the depth-scaling factor defined in Eq. (5) holds for these depths.[10] By calculating the mean electron energy $\bar{E}_d$ as a function of depth in different phantom materials we are able to find the scaling factor directly and establish whether it is constant with depth. In a related paper we show that for depths scaled to give equal mean energies, the stopping-power ratios required for dosimetry in plastic phantoms are equivalent to those in water to within a few tenths of a percent,[21,22] i.e. in effect the energy spectra are identical if the mean energies are matched.

In the following we first briefly describe the simulated clinical beams and the calculation codes used in this study. The beam parameters $\bar{E}_o$, $E_{o,p}$, R_{50} and R_p calculated using various simulated clinical beams are presented and their relationships are studied. We assess the accuracy of the energy-range relationships recommended in protocols when they are applied in realistic clinical electron beams.

We will present the number-averaged and fluence-averaged mean electron energy at the surface and at depth in a phantom as a function of off-axis distance.

We calculate the depth-scaling factors directly by scaling the depth in a non-water phantom to the water-equivalent depth where the mean energies are the same for various beams and materials and compare our calculated values with those recommended in protocols.

II. METHOD OF CALCULATIONS

A. The incident clinical beams and phantom calculations

The simulation of various accelerators and the calculation of dose distributions in a phantom are described in detail in an earlier paper.[16] The position, energy and angle of every particle emerging from the accelerator are stored in a "phase-space" data file. The energy cutoffs for particle transport are set to ECUT=0.700 MeV (total energy), AE=0.521 MeV and PCUT=AP=0.010 MeV. In all cases, the PRESTA electron algorithm[23] is employed with ESTEPE=0.01, although this value is conservative and the default value is adequate in the BEAM code.[16]

The clinical electron beam field size is 10×10 cm^2, 25×25 cm^2 and 20×20 cm^2 for beam energies 5–21 MeV, 25–40 MeV and 50 MeV respectively. The SSD is 100 cm and 110 cm for energies 5–40 MeV and 50 MeV respectively. In the BEAM simulation, the energy of electrons at the exit vacuum window of an accelerator is adjusted to match the R_{50} value of the measured and Monte Carlo calculated depth-dose curves. The dose distributions are calculated by using the EGS4 user code DOSXYZ. The comparison between calculated and measured dose distributions can be found in references 16 and 20.

The calculation of depth-dose curves in plastic phantoms was done with materials as defined in ICRU Report 37 ex-

cept for white (or high impact) polystyrene which is taken as having a density of 1.048 g/cm^3 and a TiO_2 content of 3% by weight.[10] Since ICRU Report 37 does not provide data for this material, we have used the default density effect correction in PEGS4. Unfortunately this leads to some inconsistency in the relative stopping powers.

B. Analysis of phase-space files

Two computer codes, PHSP_ENXY and PHSP_SPECXY, are used to analyze the phase-space files from BEAM to obtain the mean energy and energy spectra of simulated beams at the surface of the phantom. The codes allow the user to select particles according to the particle's history by making use of the LATCH feature of BEAM.[16]

PHSP_ENXY calculates both the number-averaged mean energy, $\bar{E}_o$, and the fluence-averaged mean energy, $\bar{E}_{o,f}$, in square strips on the phantom surface. The number-averaged energy $\bar{E}_o$ and fluence-averaged energy $\bar{E}_{o,f}$ in some region A are calculated as:

$$\bar{E}_o = \frac{\Sigma_{i=1}^{n} E_i}{n}, \tag{6}$$

$$E_{o,f} = \frac{\Sigma_{i=1}^{n} E_i (\cos\theta_i)^{-1}}{\Sigma_{i=1}^{n} (\cos\theta_i)^{-1}}, \tag{7}$$

where E_i and θ_i are the energy and the angle (relative to z-axis) of all particles in region A, and θ is capped at 89° to prevent distortion (see reference 24). The fluence-averaged mean energy, $\bar{E}_{o,f}$, is the quantity which corresponds to the mean energy scored in a phantom (see next section). The number-averaged mean energy, $\bar{E}_o$, corresponds to that measured by various instruments.

PHSP_SPECXY calculates the energy spectra in regions specified by the user at the surface of the phantom. The energy bin size of the spectrum is set by the user.

The calculated energy spectra are used to obtain the most probable energy, $E_{o,p}$, of clinical incident beams. The detailed spectra and angular distributions of all beams analyzed in this paper are presented in an internal report[20] which is available on the www (world-wide web) at http://www.irs.inms.nrc.ca/inms/irs/papers/PIRS439/pirs439.html.

C. The EGS4 user-code ENXYZ

The "phase-space" data files are used as input (incident beams) to the EGS4 user-code ENXYZ to calculate the spatial variation of the electron mean energy in the phantom. In using the code ENXYZ, Cartesian coordinates are employed and the phantom is divided into many small rectangular volume elements at the user's choice and the mean energy is calculated in each volume of interest. ENXYZ applies the techniques used in the NRCC EGS4 user-code FLURZ[25] to calculate the mean energy in phantoms. The mean energy of an electron spectrum at a position x,y,z is defined by

$$\bar{E}(x,y,z,\Delta) = \frac{\int_{\Delta}^{E_{max}} E(x,y,z)\Phi_T(x,y,z)dE}{\int_{\Delta}^{E_{max}} \Phi_T(x,y,z)dE}, \tag{8}$$

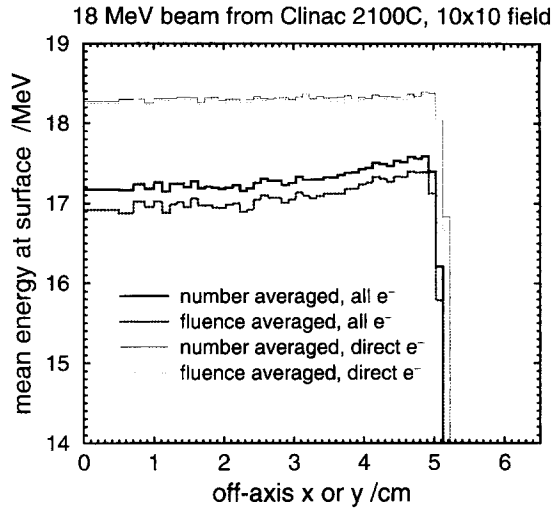

FIG. 1. Calculated electron mean energy, averaged over square rings, as a function of off-axis position at a phantom surface for an 18 MeV, 10×10 cm^2 beam from the Clinac 2100C. The average energy of all electrons near the field boundary is about 0.4 MeV higher than that near the central-axis while for direct electrons the average energy near the field boundary is only about 0.1 MeV higher than that near the central-axis.

where $\Phi_T(x,y,z)$ is the fluence spectrum of charged particles in the region of interest [i.e. $\Phi_T(x,y,z)dE$ is the fluence of charged particles with energies between E and E+dE], and Δ is the low energy cut-off (=ECUT) below which all electron histories are to be terminated. The value of Δ is set by the user. For each volume element the ENXYZ code calculates the sum of the curved path-length for each step times the mid-step energy of electrons divided by the summation of path-length of electrons in the region of interest.[24] This technique avoids any inaccuracies associated with using a binned representation of the fluence spectrum in Eq. (8). The code allows the user to exclude the effects of secondary charged particles and consider only the fluence of primary electrons. The electron histories have been calculated down to an energy Δ. The code also allows the user to make use of the LATCH feature of BEAM[16] to study the effects of scattered electrons from the beam defining system and contaminant photons when a phase-space file from BEAM is used as an incident beam.

The stopping powers used in the calculations are the ICRU Report 37 values[26] as implemented in EGS4.[27] The PRESTA electron algorithm[23] is employed in all the Monte Carlo calculations. The calculation speed is similar to that of DOSXYZ to calculate dose distributions (a few hours for a typical calculation for a beam with a 10×10 cm^2 field size and with good statistics, i.e. ±1%).

III. RESULTS OF MONTE CARLO CALCULATIONS

A. Mean energy at the phantom surface and R_{50}

The mean energy at the surface of the phantom is not precisely defined since there is a difference between the

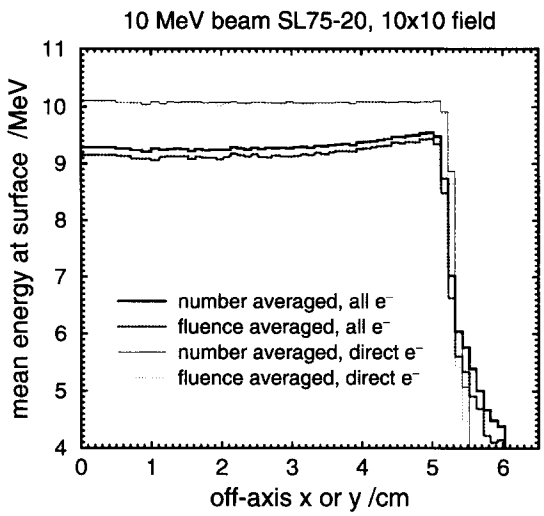

FIG. 2. Calculated electron mean energy, averaged over square rings, as a function of off-axis position at a phantom surface for a 10 MeV, 10×10 cm^2 beam from the SL75-20. The average energy of all electrons near the field boundary is about 0.3 MeV higher than that near the central-axis while for direct electrons the average energy near the field boundary is only about 0.1 MeV higher than that near the central-axis.

number-averaged mean energy [Eq. (6)] and the fluence-averaged mean energy [Eq. (7)]. In addition, the mean energy varies with off-axis positions.

Figures 1, 2 and 3 show the calculated electron mean energy above 700 keV as a function of off-axis position (in square rings) at the phantom surface for an 18 MeV beam from a Clinac 2100C, a 10 MeV beam from an SL75-20 and a 6 MeV beam from a Therac 20 respectively.

Fluence-averaged mean energy is about 2% lower than the number-averaged mean energy at the surface of the phantom due to the fact that the lower-energy electrons in the incident beam are at large angles on average.

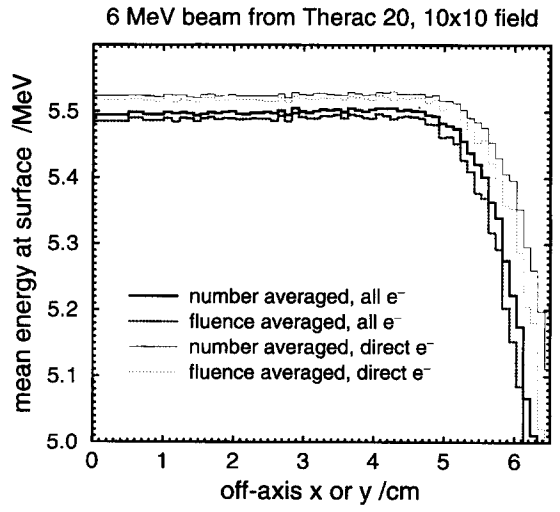

FIG. 3. Calculated electron mean energy, averaged over square rings, as a function of off-axis position at the phantom surface for a 6 MeV, 10×10 cm^2 beam from the Therac 20. There are very few electrons contributing to the average outside the field edge at 5 cm.

Note that in fig. 1 the average energy of all electrons near the field boundary is about 0.4 MeV higher than that near the central-axis while for direct electrons (those that do not hit any jaws, collimators or applicators) the average energy near the field boundary is only about 0.1 MeV higher than that near the central-axis.

Unlike the beams from the Clinac 2100C and the SL75-20 of figs. 1 and 2, the mean energies decrease slowly outside the field for a 6 MeV beam from the Therac 20 as shown in fig. 3. This is due to the design of the applicator of the Therac 20 and the larger air gap ($\approx$10 cm) between the applicator and the surface of the phantom. The decrease is more rapid for higher energy beams from the Therac 20 since there is less scattering. It should also be noted that the field edge is sharply defined and this slow drop in energy for the 6-MeV beam is for a very small number of electrons.

Table I lists the characteristics of the simulated beams and calculated $\bar{E}_0$ along with values determined according to protocols. Values of $\bar{E}_0$ presented in table I are the number-averaged mean energy at the surface of the phantom inside the field.

Incident electrons at a phantom surface in a realistic clinical beam contain scattered low-energy electrons from beam defining components and these scattered electrons decrease the average electron energy at the phantom surface but they have very little influence on the value of R_{50}. Depending on the design of an accelerator, the number of scattered electrons varies considerably[16] and it is very difficult to obtain a relationship between R_{50} and $\bar{E}_0$ for various beams from different accelerators.

Figure 4 shows the energy-range relationship for electron beams from different accelerators. The scatter in the relationship between $\bar{E}_0$ and R_{50} improves considerably when the scattered low-energy electrons are excluded from the calculation of average electron energy (as shown by the filled symbols). The relationship obtained using direct electrons is close to the result of monoenergetic beam calculations by Rogers and Bielajew[8,10] except at high energies.

Although the electrons from the high-energy scanned beams are almost monoenergetic, there are discrepancies between the results of this work and those of Rogers and Bielajew.[8] We have found that the discrepancies relate to the widely used inverse-square law correction to convert central-axis depth-dose curves for parallel incident beams to the central-axis depth-dose curves for phantoms at a finite SSD from a point source. Figure 5 shows that there is considerable difference between a 50 MeV depth-dose curve at SSD = 110 cm calculated for an idealized point source in vacuum vs the depth-dose curve calculated for an incident parallel beam and corrected using $(SSD/(SSD+d))^2$. It can be seen that the error in using the $1/r^2$ corrected parallel beam results for R_{50} or R_p in point source beams is about 3 mm. The results in the upper right corner of fig. 4 show that the difference between the results of Rogers and Bielajew[8] and the current results can be explained by this effect. This effect is

TABLE I. Comparison of values of $\bar{E}_o$, the number-averaged mean energy of electrons inside the beam on the phantom surface, as calculated for the realistic beams (for $\Delta = 189$ keV) and as determined from the value of R_{50} according to the AAPM TG-21 protocol (i.e., $\bar{E}_0 = 2.33R_{50}$) (Ref. 2), the IAEA protocol's tabulation (Ref. 4), and the tabulations of RB-86 (Ref. 8). The values of R_{50} and d_{max} are from the calculations.

Machine	$E_{nominal}$ MeV	R_{50} (cm)	d_{max} (cm)	Calculated[a] $\bar{E}_o$	Calculated[a] $\bar{E}'_o$	$\bar{E}_o$ (MeV) 2.33R_{50}	IAEA	RB-86
	6	2.63	1.4	6.11	6.52	6.13	6.24	6.61
	9	4.00	1.9	9.10	9.75	9.32	9.40	9.68
Clinac	12	5.20	2.7	11.74	12.27	12.12	12.23	12.48
2100C	15	6.50	2.1	14.59	15.34	15.15	15.25	15.54
	18	7.72	1.9	17.35	18.33	17.96	17.82	18.43
	5	2.08	1.1	5.07	5.41	4.85	4.97	5.27
	10	4.12	2.1	9.34	10.08	9.60	9.64	10.00
SL75-20	14	5.98	1.7	13.28	14.53	13.93	13.95	14.33
	17	6.96	1.9	15.28	16.67	16.22	16.32	16.64
	20	8.10	1.8	17.76	19.55	18.87	18.75	19.36
	6	2.31	1.3	5.53	5.75	5.38	5.52	5.87
KD2	11	4.21	2.5	9.70	10.06	9.81	9.82	10.23
	21	8.30	3.0	18.74	19.42	19.34	19.25	19.87
	6	2.18	1.3	5.50	5.52	5.08	5.20	5.56
	9	3.42	2.1	8.25	8.30	7.97	8.05	8.40
Therac	13	5.14	3.2	12.14	12.26	11.98	12.09	12.39
20	17	6.85	4.2	15.93	16.16	15.96	16.10	16.38
	20	8.10	4.2	18.74	19.09	18.87	18.75	19.36
	25	10.36	3.0	24.53	24.56	24.14	24.21	25.06
MM50	40	15.47	2.5	38.90	38.98	36.05	37.55	39.62
	50	18.55	2.8	48.90	49.05	43.22	46.38	49.90

[a]$\bar{E}_o$ is the average energy of all electrons inside treatment field. $\bar{E}'_o$ is the average energy of only direct electrons inside treatment field.

only important for high energies since the $1/r^2$ corrections are much less at shallow depths.

B. Most probable energy at phantom surface and R_p

The most-probable electron energy at the phantom surface, $E_{o,p}$, is not affected by the electron beam defining system. Thus it is not surprising that the relationship between $E_{o,p}$ and R_p is independent of beam quality. Figure 6 shows the relationship between most-probable energy, $E_{o,p}$, and practical range, R_p, obtained from realistic clinical beam simulations and using various formulae.[3,8,9] Despite wide differences in the energy spectra of clinical beams,[16] there is little variation in $E_{o,p}$ for a given value of R_p for beams from various accelerators. Figure 6 shows that various formulae[3,8,9] reproduce the simulated beam data with an accuracy of 3% from 5–50 MeV. For the 50 MeV beam from the MM50 accelerator, $E_{o,p}$ is underestimated by 2% and 0.7% using the ICRU formula and the analytical energy-range relationship by Sorcini and Brahme[9] respectively. The overestimation (1%) at this high energy by the relationship of Rogers and Bielajew[8] is again due to the inverse-square law correction approximation as discussed above. Table II presents a comparison of calculated and measured values of R_p and a comparison of $E_{o,p}$ values obtained from the Monte Carlo simulations (using 10 keV energy bins) and those obtained from the ICRU formula [Eq. (1)] using the Monte

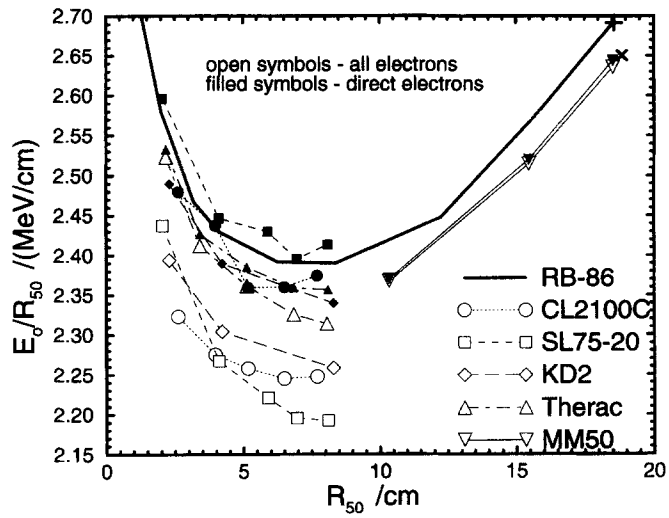

FIG. 4. Energy-range relationship for clinical electron beams as calculated for various realistic beams at an SSD of 100 cm. The open symbols are for all electrons (in the field) including scattered electrons from beam defining components, and the filled symbols are for the direct electrons (in the field) excluding those scattered electrons which have interacted with the beam defining components. At the upper right corner of the figure, the symbols + and × show the results using a $1/r^2$ corrected depth-dose curve for a 50 MeV monoenergetic parallel beam and the depth-dose curve for a 50 MeV monoenergetic point source, respectively. $\bar{E}_0$ is the number-averaged mean energy which is typically up to $1\frac{1}{2}$% higher than the fluence-averaged mean energy.

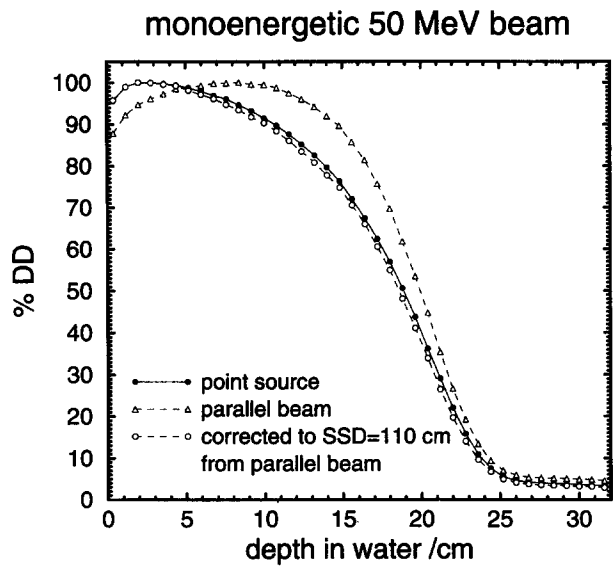

FIG. 5. Differences between the filled (correct) and open (approximate) circles show the errors introduced by using the inverse-square-law approximation to convert depth-dose curves for parallel beams to depth dose-curves for point sources for a 50 MeV monoenergetic incident beam. The incident beam field is 20×20 cm^2 in both cases and SSD is 110 cm for the point source beam. The R_{50} values are 18.87 and 18.58 cm for the point source incident beam and the parallel incident beam that has been corrected to SSD=110 cm using the inverse-square-law respectively.

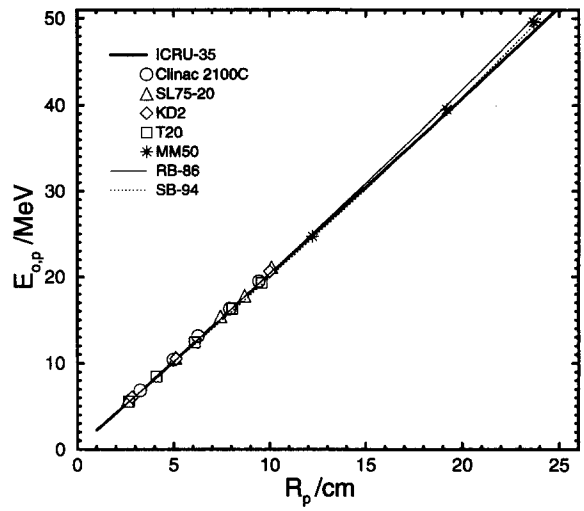

FIG. 6. The relationship between most-probable energy on the phantom surface, $E_{o,p}$, and practical range, R_p, for various clinical electron beams in a water phantom. $E_{o,p}$ and R_p of clinical beams are obtained from the spectra and calculated central-axis depth-dose curves of simulated beams. Values of RB-86 are from Monte Carlo calculations by Rogers and Bielajew (Refs. 8 and 10). Values of SB-94 are from analytical energy-range relationships by Sorcini and Brahme (Ref. 9).

Carlo calculated values of R_p. R_p is obtained from the depth-dose curves as the depth of intersection of a line drawn tangent to the depth-dose curve at the point of maximum slope and a line extrapolated from the bremsstrahlung tail. The uncertainty in values of R_p is about 1% due to the procedure for obtaining them.

The close agreement between the calculated and mea-

TABLE II. Comparison of values of the practical range, R_p, from the Monte Carlo calculations and from experiments and a comparison of values of $E_{o,p}$ obtained using the Monte Carlo simulations and those using the ICRU formula [Eq. (1)] for various clinical electron beams.

Machine	$E_{nominal}$ MeV	R_p (cm)		$E_{o,p}$ (MeV)	
		Monte Carlo	$R_p^{exp}-R_p^{MC}$	Monte Carlo	$E_{o,p}^{MC}-E_{o,p}^{ICRU}$
Clinac 2100C	6	3.26	0.00	6.88	0.18
	9	4.99	0.01	10.39	0.23
	12	6.25	0.02	13.05	0.36
	15	7.92	0.05	16.31	0.25
	18	9.44	0.12	19.49	0.36
SL75-20	5	2.60	0.03	5.66	0.28
	10	5.10	0.05	10.66	0.28
	14	7.43	−0.04	15.34	0.27
	17	8.70	-	17.79	0.15
	20	10.10	−0.20	21.04	0.57
KD2	6	2.84	0.01	6.05	0.19
	11	5.12	−0.02	10.51	0.09
	21	10.00	0.10	20.59	0.32
Therac 20	6	2.68	0.01	5.60	0.06
	9	4.10	0.01	8.42	0.04
	13	6.10	0.00	12.41	0.02
	17	8.05	0.03	16.35	0.03
	20	9.59	0.01	19.30	−0.14
MM50	25	12.23	0.10	24.77	−0.04
	40	19.20	0.12	39.50	0.34
	50	23.70	0.09	49.69	1.14

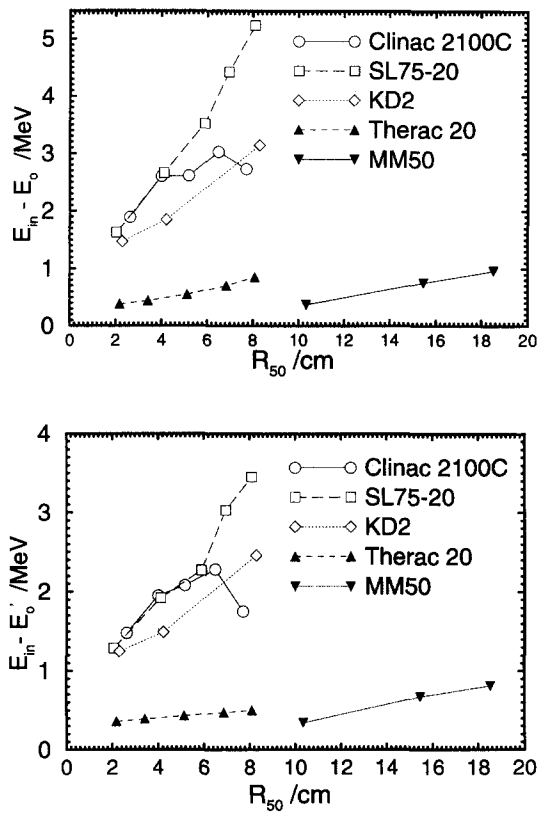

FIG. 7. Energy lost in traversing the accelerator, i.e. $E_{in}-\bar{E}_o$ and $E_{in}-\bar{E}_o'$ vs R_{50}, where $\bar{E}_o$ is the number-averaged mean energy of all electrons at the phantom surface and $\bar{E}_o'$ is the number-averaged mean energy of direct electrons at the phantom surface. The direct electrons do not include the electrons scattered from the beam defining system.

sured values of R_p shown in Table II shows that by adjusting the energy of electrons from the accelerator vacuum to match the experimental values of R_{50}, we are also accurately matching R_p values. The agreement is quite satisfactory between the most probable energies calculated with the standard (ICRU) formula based on the R_p value and the Monte Carlo values. Nonetheless, for scattering foil accelerators there is a clear trend for the Monte Carlo value to be typically 200 to 300 keV higher than the ICRU value.

C. Relationship between incident energy E_{in} and $\bar{E}_o$

The relationship between incident electron energy at the exit vacuum window of an electron beam, E_{in}, and the average electron energy at the phantom surface, $\bar{E}_o$, is influenced by the thickness of scattering foils and the design of the beam defining system of an accelerator. Figure 7 shows $E_{in}-\bar{E}_o$ and $E_{in}-\bar{E}_o'$ vs R_{50} for various clinical beams, where $\bar{E}_o'$ is the average energy of direct electrons at the phantom surface. These direct electrons are not influenced by the design of beam defining system. It can be seen that the difference between E_{in} and $\bar{E}_o$ or $\bar{E}_o'$ is small (<1 MeV) for beams from the Therac 20 (which are scanned beams with no scattering foils) and from the MM50 accelerator (which produces scanned beams and has a very thin scattering foil). In the accelerators with scattering foils, the main reason that the energy loss increases with energy is that the scattering foils generally get thicker with higher energy.

ICRU Report 35[3] gives an approximate formula to relate $\bar{E}_o$ to E_{in}:

$$\bar{E}_o = E_{in} - \Sigma(\Delta E)_{tot,n} \tag{9}$$

where $(\Delta E)_{tot,n}$ is the mean total energy loss in layer n of material being traversed, i.e., the sum of collision and radiative energy losses. Since each side in Eq. (9) can be calculated using the simulated clinical beams, we can assess the accuracy of this formula. This is an idealized case because both calculations are known to use identical descriptions of the scattering foils.

Figure 8 shows the discrepancies between $E_{in}-\bar{E}_o$ and calculated $\Sigma(\Delta E)_{tot,n}$ for various beams from different medical accelerators (filled symbols). The calculated energy loss in the intervening material layers is given by $\Sigma(\Delta E)_{tot,n} = \Sigma dt_n(dE/dt)_n$. It can be seen (fig. 8) that the discrepancies are small (<0.4 MeV) for a variety of clinical beams although they range between 600 keV high and 700 keV low. This amounts to only $\pm 4\%$ of the beam energy, but represents an error in the estimated energy loss of over 20% in some cases. Figure 8 also shows the discrepancies between the incident energy and the mean energy of the direct electrons in the field, $E_{in}-\bar{E}_o'$ and the calculated estimate, $\Sigma(\Delta E)_{tot,n}$ (open symbols). One might expect that these discrepancies should be smaller, however they are larger for beams from accelerators with scattering foils. This is because the simple model of Eq. (9) assumes that all electrons reach the patient plane. In reality, and in the Monte Carlo calculations, those electrons which undergo large energy-loss events are more likely lost from the beam and hence the electrons left in the beam have a higher average energy. By including the electrons scattered from the beam defining system, the model works better. That this model works at all is because secondary electrons in the beam play little role in the average energy. We have studied the effect of secondaries on the average energy. The results show that for the 6 and 18 MeV electron beams from the Clinac 2100C only 0.8% and 1.7% of the total electrons inside the field are secondary electrons with average energies of 1.45 and 3.11 MeV respectively. By excluding these secondaries, the average energy would increase by 0.65% (0.04 MeV) and 1.7% (0.25 MeV) for the 6 and 18 MeV beams from the Clinac 2100C respectively.

D. Mean energy as a function of depth for monoenergetic incident electron beams

For incident monoenergetic electron beams Fig. 9 compares the mean energy of primary electrons as a function of depth calculated with the code ENXYZ to those calculated by Andreo and Brahme and used in the IAEA Code of Practice[17,4] and to those predicted by the Harder formula and used in the AAPM TG-21 protocol. Our results using monoenergetic incident beams and considering only primary electrons in the medium agree reasonably well with values

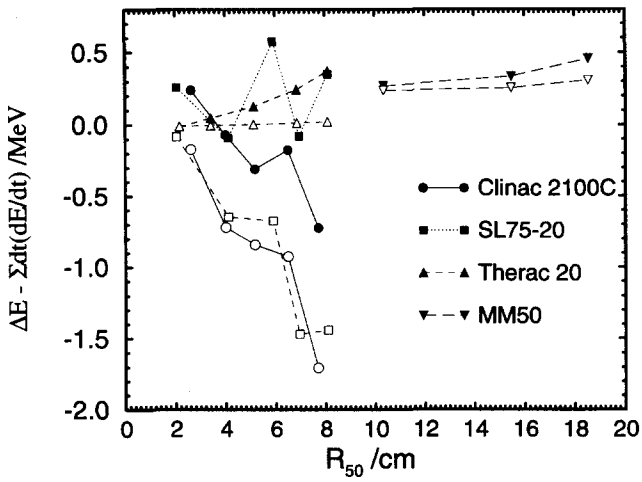

FIG. 8. The difference between the actual energy loss in the accelerator and the simple estimate given by Eq. (9), i.e. $\Delta E - \Sigma dt(dE/dt)$ vs R_{50}, where filled symbols correspond to $\Delta E = E_{in} - \bar{E}_o$ and open symbols correspond to $\Delta E = E_{in} - \bar{E}'_o$ where $\bar{E}'_o$ is the average energy of direct electrons at the phantom surface. The direct electrons do not include the electrons scattered from the beam defining system.

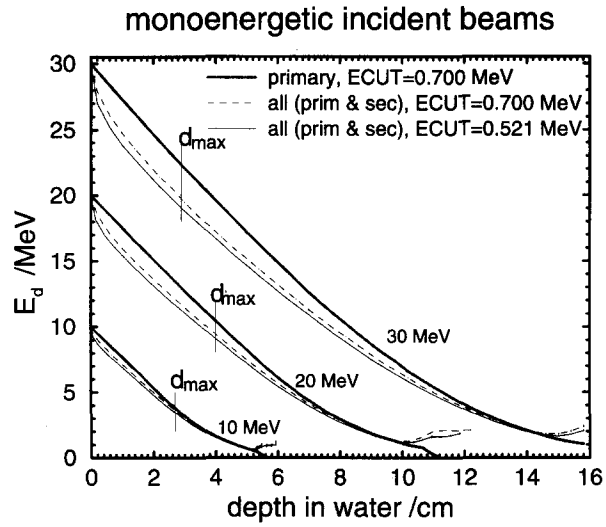

FIG. 10. Comparison, for incident monoenergetic beams, of the calculated mean energy as a function of depth in a water phantom for just the primary electrons or for both primary and secondary electrons. For calculations including secondary electrons, results are shown for electrons with energies down to 521 or 700 keV total energy (10 or 189 keV kinetic energy).

calculated by Andreo and Brahme[17,4] despite the differences in the Monte Carlo models used in the calculations (different codes and point source vs parallel beams). The maximum differences in calculated mean energies are 0.15 MeV (1.5%), 0.3 MeV (1.5%) and 0.5 MeV (1.7%) for 10 MeV, 20 MeV and 30 MeV incident beams respectively. The discrepancies are reduced by a factor of two if parallel incident beams are used in our calculation as was done by Andreo and Brahme.

As shown in Fig. 10, we have calculated mean energies as a function of depth in a water phantom for several further cases with 10, 20 and 30 MeV monoenergetic incident beams. In case 1, only primary electrons are considered in the calculation, as in fig. 9. In case 2, both primary and secondary electrons are considered but those secondary electrons created from photons are not included. In case 3, all electrons are considered. In case 4, the electron cut-off energy, ECUT=0.521 MeV (total electron energy), is used in the calculation instead of ECUT=0.700 MeV (total electron energy) as in all other calculations. It can be seen that:

- There is a significant drop in mean energy when secondary electrons are included in the averaging, especially at shallow depth. The decrease at d_{max} is 5%, 10% and 13% for 10 MeV, 20 MeV and 30 MeV beams respectively. At the tail there is an increase in the mean energy because only photons create secondary electrons beyond R_p.
- Changing ECUT from 0.700 MeV to 0.521 MeV has a small but not negligible effect on the calculated mean energy of all electrons. The further decrease in mean energy at d_{max} is 4.7%, 3.7% and 3.6% for 10 MeV, 20 MeV and 30 MeV beams respectively.

It is found by calculation that although knock-on electrons created by phantom-generated bremsstrahlung photons play some role past R_p, they play no role in the mean energy over the entire therapeutic depth (not shown). This is because it is a second order effect. It is also found that the calculated mean energy of primary electrons is not sensitive to a change of ECUT from 0.700 MeV to 0.521 MeV. The curve with ECUT=0.521 (not shown) is virtually identical to that with ECUT=0.700 MeV. This is because there are very few primary electrons with energies below 0.700 MeV.

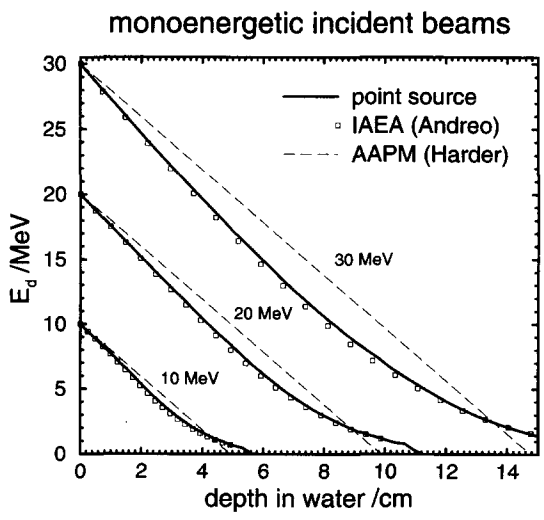

FIG. 9. Comparison of the mean energy of primary electrons calculated with the code ENXYZ (for a point source at an SSD of 100 cm) to those calculated by Andreo and Brahme (Ref. 17) for a broad parallel beam [recommended in the IAEA Code of Practice (Ref. 4)] and to those calculated using Harder's relation employed in the AAPM TG-21 protocol (Ref. 2).

E. Mean energy as a function of depth for incident clinical electron beams

In protocols for clinical electron beams, the determination of the mean energy at depth in a water phantom, $\bar{E}_d$, is based

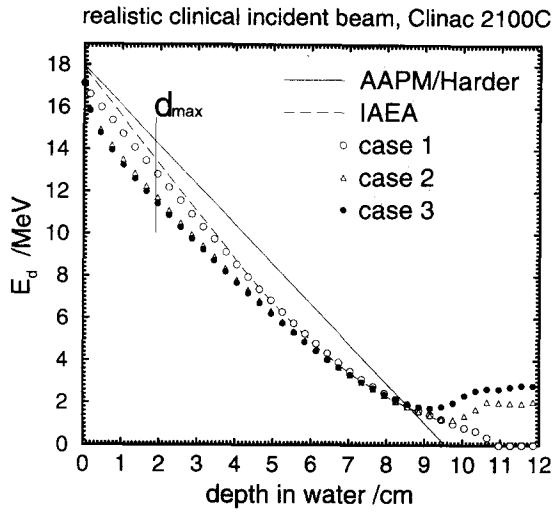

FIG. 11. Comparison of values of mean energy as a function of depth as calculated by Monte Carlo and those obtained from protocols for the 18 MeV beam from a Clinac 2100C accelerator. In case 1, only electrons are included in the realistic incident beam and only primary electrons are considered in the water phantom. In case 2, only electrons are included in the realistic incident beam and both primary and secondary electrons are considered in the water phantom. In case 3, both electrons and contaminant photons are included in the realistic incident beam and both primary and secondary electrons are considered in the water phantom.

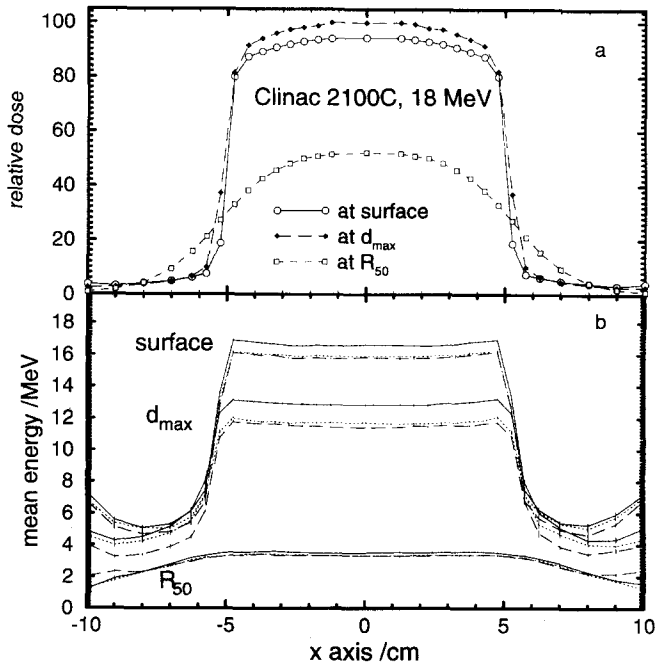

FIG. 12. (a) Monte Carlo calculated dose profiles and (b) mean-energy profiles at different depths in a water phantom for an 18 MeV beam from the Clinac 2100C. In the lower panel, solid lines are the mean energy of primaries in phantom and only including electrons in the incident beams. Dotted lines are the mean energy of both primary and secondary electrons and only including electrons in the incident beams. Dashed lines are the mean energy of both primary and secondary electrons and including electrons and contaminant photons (i.e. the complete realistic beam).

on two beam parameters, $\bar{E}_o$ and R_p. In the AAPM TG-21 protocol, $\bar{E}_o$ is determined from the relationship $\bar{E}_o = 2.33R_{50}$ while in the IAEA Code of Practice, $\bar{E}_o$ is tabulated vs R_{50}. The mean incident electron energies determined according to the AAPM and the IAEA protocols for each beam are shown in table I. In addition to the difference in $\bar{E}_o$ values determined according to the two protocols, the AAPM protocol[10] uses a simple formula, $\bar{E}_d = \bar{E}_o(1 - d/R_p)$ while the IAEA Code of Practice[4] gives values tabulated as a function of $\bar{E}_o$ and d/R_p.

Figure 11 shows a comparison between our calculated values and those obtained from protocols for electron mean energy along the central axis for an 18 MeV beam from a Clinac 2100C accelerator. It can be seen in the figure and in table I that $\bar{E}_o$ determined according to protocols is 0.5 MeV (3%) higher than we calculate for the 18 MeV beam from a Clinac 2100C. This leads to an overestimation of $\bar{E}_d$ by the protocols over the entire therapeutic depth. At d_{max}, $\bar{E}_d$ is overestimated by 20% or 15% for this beam using the AAPM or IAEA protocols respectively. To study the discrepancy in detail we also calculated three different cases as shown in fig. 11. By comparing cases 1 and 2 it is seen that $\bar{E}_d$ is significantly lower when secondary electrons are included in the calculation, especially at shallow depth. By comparing cases 2 and 3, it is clear from fig. 11 that contaminant photons in the realistic beam have a negligible influence on $\bar{E}_d$.

Figure 12 shows both dose profiles and the electron mean energy profile at different depths (surface, d_{max} and R_{50}) in a water phantom for the same beam as in fig. 11. Mean energies are slightly higher (1%–3%) near the field edges than near the central axis at all depths due to scattered electrons in water phantoms and in the beam as we discussed in section III A. The mean energy shows a roughly flat distribution across the field and drops quickly beyond the treatment field. Note that with this sudden change in electron energy at the field edge, the stopping-power ratio needed to relate an ion chamber reading to the absorbed dose to water would increase by roughly 7% although since the dose is also dropping quickly, the net effect would be a small error relative to the maximum dose in the phantom at the field edge.

Figure 13 compares the calculated $\bar{E}_d$ with values determined according to the AAPM and the IAEA protocol for four clinical electron beams with incident energy range from 5 to 50 MeV. It can be seen that the discrepancies vary with beam energies as well as the depths. For a 5 MeV beam from an SL75-20 at d_{max}, $\bar{E}_d$ is overestimated by 15% according to the AAPM protocol and overestimated by 5% according to the IAEA protocol. For the 10 MeV beam from an SL75-20 at d_{max}, $\bar{E}_d$ is overestimated by 26% or 10% according to the AAPM or the IAEA protocol respectively. For a 21 MeV beam from a KD2 at d_{max}, $\bar{E}_d$ is overestimated by 30% or 18% according to the AAPM or the IAEA protocol respectively. For a 50 MeV beam from MM50 at d_{max}, $\bar{E}_d$ is overestimated by 8% according to AAPM or IAEA protocol. These discrepancies are due to our use of more sophisticated

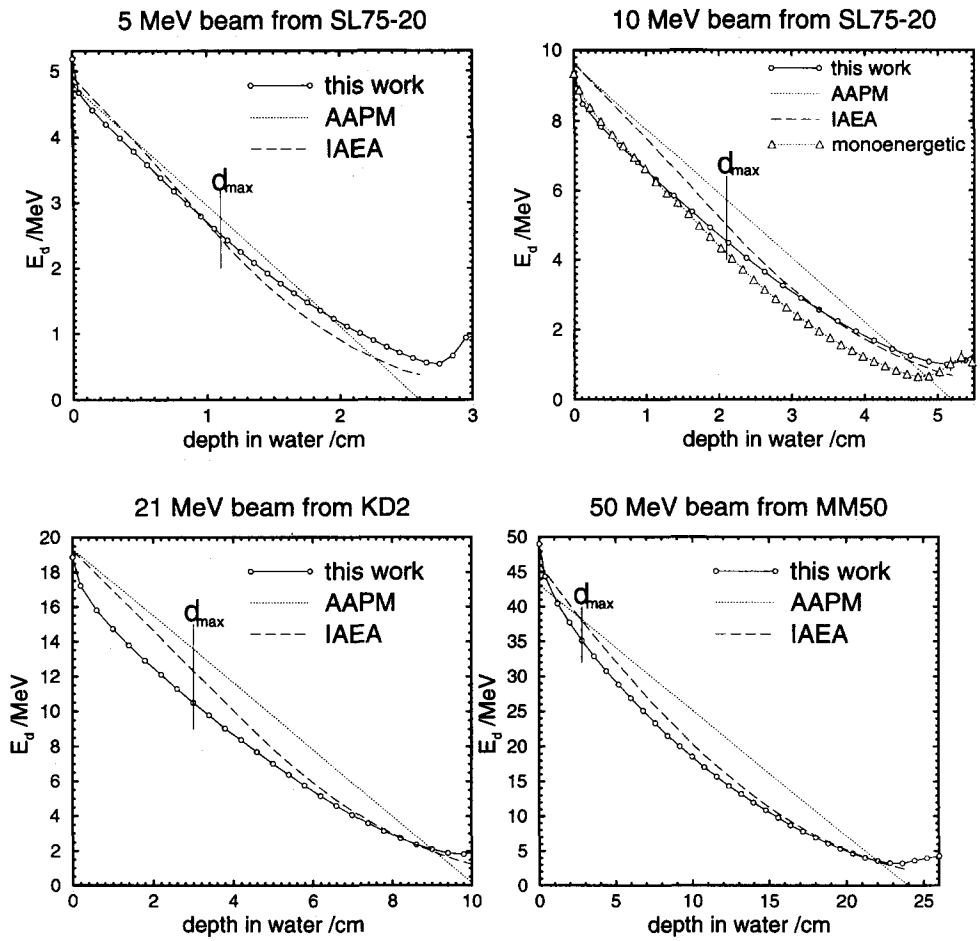

FIG. 13. Comparison between calculated $\bar{E}_d$ for full beams with $\Delta = 189$ keV and that from protocols for 5, 10, 21 and 50 MeV clinical electron beams. In the right upper panel the electron incident energy of the monoenergetic point source is 9.34 MeV which is the same as the calculated mean energy of the 10 MeV beam from the SL75-20.

models which include secondary electrons and due to the problems in how the protocols assign the mean energy at the surface.

In fig. 13, we also present our calculated $\bar{E}_d$ values for a monoenergetic incident beam with an incident energy which is the same as the calculated mean energy for the 10 MeV beam from the SL75-20. The results show that $\bar{E}_d$ for the monoenergetic beams drops more slowly than that of the clinical incident beam near the phantom surface and then it drops more quickly than that of the clinical incident beam. The lower-energy electrons in the incident clinical beam generally have a large incident angle and are more easily scattered inside the phantom, and thus have a stronger effect near the surface. Also, at large depths, $\bar{E}_d$ is dominated by the high-energy electrons in the clinical beam because the lower-energy electrons can not reach there and thus the average energy is higher at depth in the clinical beam, given that the initial mean energies are the same. This result is consistent with those of the study by Udale-Smith.[15]

Generally speaking, if $\bar{E}_0$ is overestimated according to the protocols, $\bar{E}_d$ will be underestimated over the entire therapeutic depth for any beam. If $\bar{E}_0$ is underestimated according to the protocols, the discrepancies between calculated values of $\bar{E}_d$ and those determined according to protocols, vary with the amount of underestimation of $\bar{E}_0$. In the case of the 5 MeV beam from an SL75-20 accelerator, $\bar{E}_0$ is underestimated by 2% according to IAEA protocol. This leads to a 3% underestimation of $\bar{E}_d$ at d_{max}. In the case of the 50 MeV beam from a MM50 accelerator, the IAEA Code of Practice underestimates the value of $\bar{E}_0$ by 5%. This leads to only an 8% overestimation of $\bar{E}_d$ at d_{max}.

In most cases, $\bar{E}_0$ is underestimated using the relationship $\bar{E}_0 = 2.33R_{50}$. However, this underestimation in $\bar{E}_0$ actually reduces the discrepancy between our calculated values of $\bar{E}_d$ at d_{max} and those determined according to protocols.

F. Depth-scaling factors for non-water phantoms

Figure 14 shows the calculated depth-dose curves and mean energies along the central-axis in different phantom materials for the same 18 MeV incident electron beam from the University of Wisconsin Clinac 2100C. If we scale the depth (in cm) in non-water materials to the water-equivalent depth (in cm) such that the mean electron energy is the same

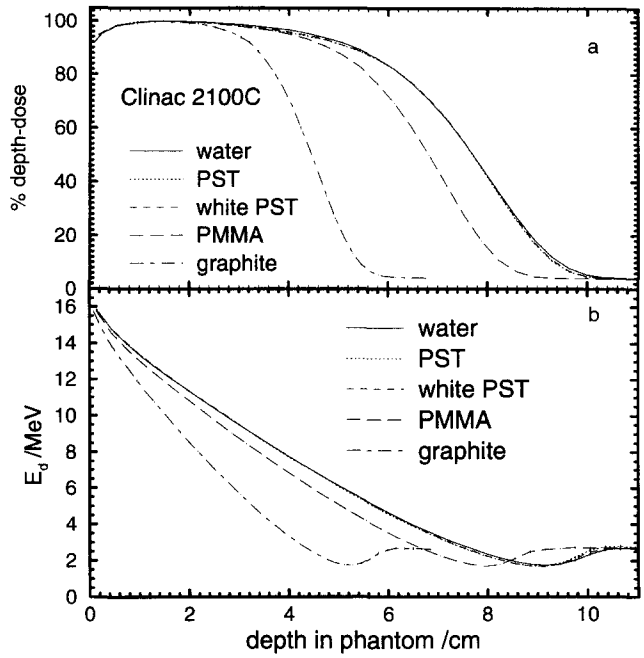

FIG. 14. Calculated central-axis depth dose curves and mean energies $\bar{E}_d$ as a function of depth in different phantom materials for an 18 MeV beam from the Clinac 2100C. The values of the mass density used in the calculation are: $\rho_{\text{polystyrene}}=1.060$ g/cm^3, $\rho_{\text{white polystyrene}}=1.048$ g/cm^3, $\rho_{\text{PMMA}}=1.190$ g/cm^3 and $\rho_{\text{graphite}}=2.00$ g/cm^3. The ECUT used in the calculation is 0.700 MeV.

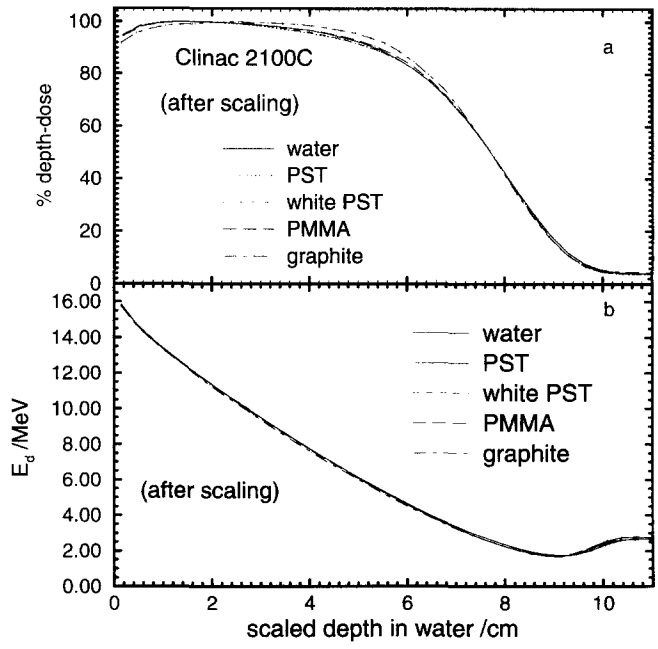

FIG. 15. Calculated depth-dose curves and $\bar{E}_d$ values for different media for an 18 MeV beam from the Clinac 2100C after scaling to the water equivalent depth using the depth-scaling factors, i.e. effective density, ρ_{eff}, given in table III.

at corresponding depths, we find that the depth-scaling factor is equal to R_{50}(in water)/R_{50}(in medium). This is just the definition of the effective density in the AAPM TG-25 protocol.[10] After scaling the depth in the non-water materials to the equivalent depth in water, the resulting depth-dose curves are shown in Fig. 15. The discrepancies between the depth-dose curves in water and the scaled depth-dose curves in plastics are less than 1% of the maximum dose. This indicates that the spectra are also similar at the scaled depths. The discrepancies between the depth-dose curve in water and the scaled depth-dose curve in graphite are up to 3%.

The good agreement for the scaled mean energies over the entire depth range shows that the scaling factor is a constant with depth. Although our scaling factor has the same formula as that of the effective density defined by the AAPM TG-25 protocol, as shown in table III, our values are different from the values recommended in the AAPM TG-25 protocol. For example, the AAPM recommended value of effective density for clear polystyrene is 0.975 while ours is 1.001. There is a 2.6% difference. The mass density of polystyrene which we used is 1.06 g/cm^3 (from ICRU Report 37) which is slightly larger than the value 1.045 g/cm^3 given in the AAPM TG-25 protocol, i.e. the mass density contributes a 1.4% difference. Therefore the values of depth-scaling factor recommended by the AAPM TG-25 protocol for clear polystyrene is underestimated by 1.2% for the 18 MeV beam. However this recommended value for clear polystyrene in the AAPM protocol is accurate for a 6 MeV beam. It is also clear from table III that there are considerable variations in effective density, both the definition and the recommended values.

The range scaling values recommended in the IAEA Code of Practice[4] are based on the ratio of continuous-slowing-down ranges [Eq. (4)] with values from ICRU Report 35, which differ by up to 0.2% from the values based on ICRU Report 37[26] values which are used everywhere else in the Code. These values generally overestimate our calculated depth-scaling factors by 1%–2% for clear polystyrene or PMMA phantoms (off scale in fig. 16).

To investigate the influence of beam energy and quality on the depth-scaling factors we calculated the factors for a variety of beams from various accelerators with nominal beam energies from 5 to 50 MeV. In Fig. 16, the calculated depth-scaling factors (or effective densities) are plotted as a function of R_{50} in plastic. It can be seen that the variation of depth-scaling factors is small ($<1.5\%$) for beam energies in the range 5–50 MeV and that the calculated depth-scaling factors have little variation with beam quality. We do a least-square-fit of the calculated data points for each phantom material to:

$$\rho^p_{eff}=A_p+B_p(R^p_{50})^2+C_p\sqrt{R^p_{50}}, \tag{10}$$

where ρ^p_{eff} is the fitted depth-scaling factor for plastic p and A_p, B_p and C_p are the fitting parameters. The values of fitted parameters for the three plastics are given in table IV and the fitted curves are shown in fig. 16. Table IV also gives the fitted coefficients for use with R_{50} in water, i.e.:

$$\rho^p_{eff}=A'_p+B'_p(R^w_{50})^2+C'_p\sqrt{R^w_{50}}. \tag{11}$$

We also calculate the depth-scaling factors for monoener-

TABLE III. Densities and effective densities or depth-scaling factors for scaling the depth (in cm) in a non-water phantom to the equivalent depth in a water phantom for an 18 MeV electron beam from a Clinac 2100C.

Material	ρ (g/cm^3)		Scaling-factor ρ_{eff}		Scaling factor
	ours[a]	AAPM[b]	ours[c]	AAPM[d]	IAEA[e]
Polystyrene	1.060	1.045	1.001	0.975	1.017
White PST	1.048	1.055	0.999	0.99	-
PMMA	1.190	1.18	1.132	1.115	1.144
Graphite	2.000	-	1.729	-	-

[a]Used in the Monte Carlo calculations, taken from ICRU37 (Ref. 26).
[b]Given in the AAPM TG-25 protocol (Ref. 10).
[c]Calculated using calculated values of R_{50} and the definition ρ_{eff} = R_{50}(in water)/R_{50}(in medium) with an 18 MeV beam from Clinac 2100C (Ref. 10).
[d]Recommended in the AAPM TG-25 protocol (Ref. 10), these are independent of $\bar{E}_o$.
[e]Recommended in the IAEA Code of Practice where the mass densities are same as those used in our calculation. Since the tabulated values given in the IAEA Code of Practice depend on $\bar{E}_o$ [1.027−0.997 (polystyrene) and 1.149−1.133 (PMMA) for $\bar{E}_o$ from 5–50 MeV respectively] we choose the value corresponding to $\bar{E}_o$ = 15 MeV which is close to the beam we used in the calculation.

getic point source incident beams for electron energies of 6, 10, 16 and 20 MeV. The calculated values of the depth-scaling factor as a function of R_{50} for monoenergetic beams are in a close agreement with those for realistic incident beams for the three plastics studied (not shown). This result further confirms that the calculated depth-scaling factors are independent of the beam quality but vary with beam energy. After scaling to common densities, our results of depth-scaling factors agree with the Monte Carlo calculations using monoenergetic beams by Grosswendt and Roos[18] within their stated uncertainties of the calculation, although they did not explicitly report their depth-scaling factors.

To study the influence of density variations for a practical non-water phantom we change the density of a plastic phantom by 16% and calculate the depth-dose and mean energy vs depth curves for the 18 MeV beam from a Clinac 2100C, as shown in Fig. 17. It can be seen that the influence of density variation has been included if the depth-scaling factor of $R_{50}^{water}/R_{50}^{plastic}$ is applied. This indicates that the influence of density variation is negligible as long as the measured values of R_{50} in water and plastic are used for the depth-scaling.

If our calculated values shown in fig. 16 are used instead of measured R_{50} values in water and in plastic, and if the mass density of the plastic used in the measurement is different from the one used in our calculations, the depth-scaling factor must be corrected by using:

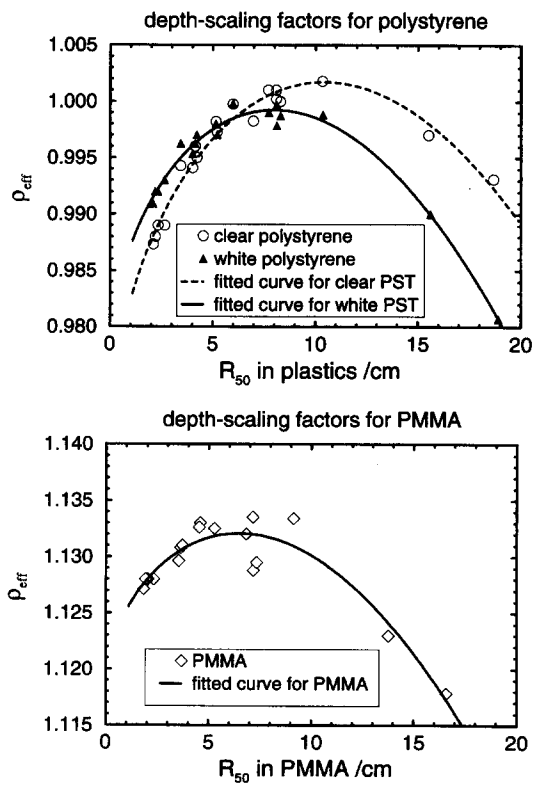

FIG. 16. Monte Carlo calculated depth-scaling factors as a function of R_{50} in plastic for clear polystyrene, white polystyrene and PMMA phantoms using clinical incident electron beams. The depth-scaling factor is calculated to ensure the mean energies are matched at equivalent depths. The densities for which these factors apply are given in table III and Eq. (12) should be used to account for variations from these values.

TABLE IV. Fitted parameters for the depth-scaling factor or effective density, ρ_{eff}^{p} by which the depth (in cm) in a plastic phantom is multiplied to give the equivalent depth in a water phantom [Eq. (5)]. Parameters are given for $\rho_{eff}^{p}=A_p+B_p(R_{50}^{p})^2+C_p\sqrt{R_{50}^{p}}$ [Eq. (10)] as a function of R_{50}^{p} for clear-polystyrene, white polystyrene and PMMA phantoms with densities as given in Table III. For other densities, the value of ρ_{eff}^{p} must be scaled using Eq. (12). The table also contains the parameters for determining the value of ρ_{eff}^{p} as a function of R_{50}^{w} from the equation $\rho_{eff}^{p} = A_p' + B_p'(R_{50}^{w})^2 + C_p'\sqrt{R_{50}^{w}}$.

Phantom materials	A_p	B_p (cm^{-2})	C_p (cm$^{-1/2}$)
Clear polystyrene	0.9688	-1.009×10^{-4}	1.360×10^{-2}
White polystyrene	0.9765	-1.184×10^{-4}	1.070×10^{-2}
PMMA	1.1179	-1.122×10^{-4}	7.416×10^{-3}
	A_p'	B_p'	C_p'
Clear polystyrene	0.9689	-1.016×10^{-4}	1.356×10^{-2}
White polystyrene	0.9762	-1.232×10^{-4}	1.092×10^{-2}
PMMA	1.1177	-9.008×10^{-5}	7.096×10^{-2}

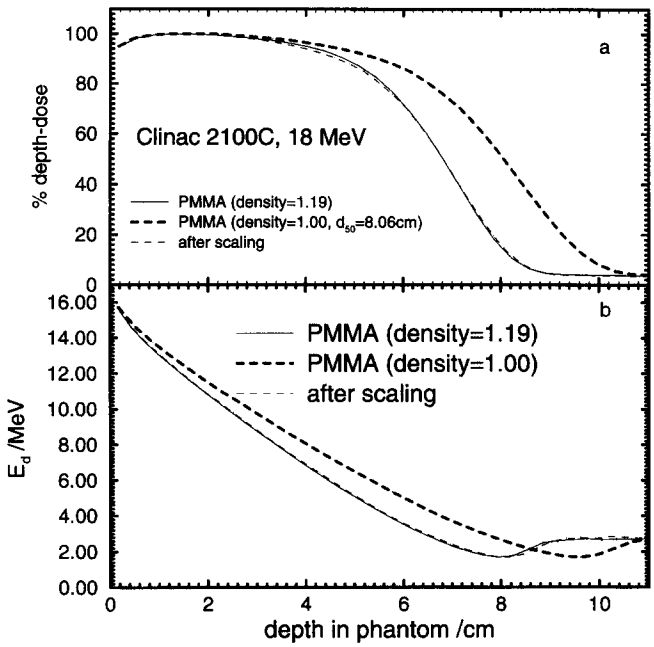

FIG. 17. Calculated depth-dose curves curves and $\bar{E}_d$ using PMMA with a different density and applying the scaling factor $\rho_{eff} = R_{50}(\text{density} = 1.19)/R_{50}(\text{density} = 1.00)$ for the 18 MeV beam from a Clinac 2100C.

$$\rho_{eff}^{usr} = \rho_{eff}^{p} \times \frac{\rho_{usr}^{plastic}}{\rho_{nom}^{plastic}}, \tag{12}$$

where ρ_{eff}^{p} is the value from Eq. (10) (fig. 16), and $\rho_{usr}^{plastic}$ and $\rho_{nom}^{plastic}$ are the mass densities of the plastics used in user's measurements and in our calculations respectively. For the above extreme case of changing the mass density of the PMMA from 1.19 to 1.00 g/cm^3, Eq. (12) gives the value of depth-scaling factor as $1.132 \times 1.00/1.19 = 0.951$ which is 0.7% less than the value obtained from the ratio of $R_{50}^{water}/R_{50}^{plastic} = 7.72/8.02 = 0.958$. However, in clinical practice the variation in density of a given type of plastic is usually less than 2% to 3%. Thus the discrepancies caused by using Eq. (12) will be very small (<0.1%).

In this study we have determined the depth-scaling factors by insisting on matching mean energies at equivalent depths. As mentioned above, this is just a stand-in for the real goal which is to match depths at which stopping-power ratios are identical, and elsewhere this has been demonstrated to be the case.[21]

The above scaling factors, while deduced in terms of mean energies at depth, can also be used as range scaling factors as can be seen by the close agreement of the entire depth-dose curves in fig. 15.

IV. CONCLUSIONS

We have presented detailed data about the mean energies at the surface of the phantom for the simulated clinical beams from a variety of medical accelerators including a Varian Clinac 2100C, a Philips SL75-20, a Siemens KD2, an AECL Therac 20 and a Scanditronix Medical Microtron 50. We have presented the mean electron energy at the surface of the phantom as a function of off-axis distance as well as the differences between the number-averaged and the fluence-averaged mean energy. It is shown that the mean energy near the field boundary is about 2% higher than that near the central-axis and that fluence-averaged mean energy is about 2% lower than that of number-averaged mean energy at the surface of the phantom. We have studied $\bar{E}_o$ and $E_{o,p}$ and their relationship with R_{50} and R_p for beams in the energy range 5–50 MeV. It is impossible to obtain a universal and highly accurate relationship between R_{50} and $\bar{E}_o$ because the number of scattered low-energy electrons varies with the machine's treatment head design. However, there exists an approximate relationship between R_{50} and $\bar{E}_o'$, the mean energy of direct electrons. This relationship is in close agreement with the energy-range relationships calculated using monoenergetic beams by Rogers and Bielajew[8] except at very high energies. Here the simple $1/r^2$ technique to calculate depth-dose curves for a point source from depth-dose curves for a parallel beam is shown to break down and explicit calculations with a point source are required.

We have shown that the empirical formula used by the AAPM and IAEA protocols to predict the most probable energy in the electron beam, viz. $E_{o,p} = 0.22 + 1.98R_p + 0.0025R_p^2$, is accurate for clinical beams with energies from 5 to 50 MeV. This formula reproduces the calculated data from realistic simulated clinical beams with an accuracy of 3%.

The electron mean energy, $\bar{E}_d$, as a function of depth is calculated in water as well as plastic phantoms. $\bar{E}_d$, calculated using realistic beams, is compared both with Harder's relationship, $\bar{E}_d = \bar{E}_o(1 - d/R_p)$, employed in AAPM protocols and with values determined according to the IAEA Code of Practice. The conventional relations generally overestimate $\bar{E}_d$ over the entire therapeutic depth. For example, the AAPM or IAEA overestimates $\bar{E}_d$ by up to 20% or 15% respectively for an 18 MeV beam from the University of Wisconsin's Clinac 2100C at d_{max}. It is also found that at all depths mean energies are 1%–3% higher near the field edges than on the central axis. The differences in the mean energies between those calculated using clinical beams and those determined according to protocols vary with the beam quality. Discrepancies in $\bar{E}_d$ decrease when the beam's mean energy $\bar{E}_o$ is underestimated by using the simple relationship $\bar{E}_o = 2.33\ R_{50}$ Eq. (2).[2,10,4]

The differences in the mean energies between those calculated using clinical beams and those determined according to protocols reflect that:

- AAPM's simple formula, $\bar{E}_d = \bar{E}_o(1 - d/R_p)$, is not accurate;
- IAEA's values are calculated using monoenergetic beams and only primary electrons are considered in the calculations;
- scattered low-energy electrons from the beam defining system in a clinical beam tend to lower the incident beam's mean energy for a given value of R_{50}.

At d_{max} the value of $\bar{E}_d$ determined according to the IAEA

Code of Practice is up to 1 MeV lower than that determined according to the AAPM protocol, depending on the beam energy as well as beam quality. It should be emphasized that in both protocols, $\bar{E}_d$ is only used to specify which fluence correction factors to use since these factors, which only apply at d_{max}, were originally specified this way. Thus, at the practical level, if more accurate values of $\bar{E}_d$ are used in clinical situations, the original data must also be re-analyzed using the more accurate data. However the IAEA Code of Practice has provided improved values of $\bar{E}_d$ without modifying the original data for fluence correction factors.[28] This inconsistency leads to only a 0.1% error in electron fluence correction factors determined according to the IAEA Code of Practice. This error is small compared to the other uncertainties in the fluence correction factor.

Using the same incident clinical beam we calculate mean energy in different non-water phantoms. The scaling factors used to convert depth in plastic to water-equivalent depth are obtained. By scaling the depth in the non-water medium to the depth in water where the mean energies are equal, we are able to obtain the scaling factor directly. The depth-scaling factor is found to be a constant as a function of depth with a small variation ($<1.5\%$) depending on the incident beam energies. The calculated depth-scaling factor is found to be equal to $R_{50}^{water}/R_{50}^{plastic}$ which is consistent with the AAPM definition of effective density. However the discrepancies between our calculated values and those recommended by the AAPM and the IAEA protocols are up to 2%. The values of the depth-scaling factor obtained by using the ratio of the continuous-slowing-down ranges employed in the IAEA Code of Practice are shown to be inaccurate and overestimate our calculated values by up to 1%–2% in all cases.

Our calculated values of depth-scaling factor for three plastics are shown in fig. 16 and parameterized in table IV. If the mass density of the user's plastic phantom is different from what we used in the calculation, Eq. (12) should be used to correct for this density effect. The curves in fig. 16 can also be used for range scaling, e.g. to determine R_{50} in a water phantom from a measured value in a plastic phantom or vice versa.

ACKNOWLEDGMENTS

We wish to thank Dr. Joanna Cygler of the Civic Hospital in Ottawa for providing the information needed to simulate the Therac 20 and the Siemens KD2, Dr. Chen Chui of Memorial Sloan-Kettering Cancer Center in New York for providing the information needed to simulate the Racetrack Microtron treatment head, Dr. Jack Janssen and Dr. Henk Huizenga of the Dr. Daniel den Hoed Cancer Clinic for information related to the Siemens KD2, and Dr. Alex Bielajew for supporting the EGS4 system at NRC. We wish to thank our colleagues Dr. Carl Ross and Dr. Charlie Ma for their valuable comments on the manuscript. One of the authors (G.X.D.) is the recipient of the MRC Studentships Award and is grateful to the Medical Research Council of Canada for providing the support. This research was partially supported by NCI Grant No. RO1 CA52692.

[a]Department of Physics, Carleton University, Ottawa, Canada. Present address: Medical Physics Department, Ottawa Regional Cancer Centre, 190 Melrose Ave., Ottawa, Ontario K1Y 4K7, Canada. Electronic mail: gding@irs.phy.nrc.ca

[b]Electronic mail: dave@irs.phy.nrc.ca

[c]Author Note: digital data for figures are available at: http://www.irs.inms.nrc.ca/inms/irs/papers/ENERGYGD/energygd.html

[1]NACP, "Procedures in external beam radiotherapy dosimetry with photon and electron beams with maximum energies between 1 and 50 MeV," Acta Radiol. Oncol. **19**, 55–79 (1980).

[2]AAPM Task Group-21, "A protocol for the determination of absorbed dose from high-energy photon and electron beams," Med. Phys. **10**, 741–771 (1983).

[3]ICRU, "Radiation dosimetry: Electron beams with energies between 1 and 50 MeV," ICRU Report 35, Bethesda MD (1984).

[4]International Atomic Energy Agency (IAEA), *Absorbed Dose Determination in Photon and Electron Beams; An international Code of Practice,* Technical Report Series No. 277 (IAEA, Vienna, 1987).

[5]A. Brahme, T. Kraepelien, and H. Svensson, "Electron and photon beams from a 50 MeV racetrack microtron," Acta Radiol. Oncol. **19**, 305–319 (1980).

[6]B. Markus, "Beitrage zur Entwicklung der Dosimetrie schneller Elektronen," Strahlentherapie **116**, 280–286 (1961).

[7]M. J. Berger and S. M. Seltzer, "Quality of radiation in water medium irradiated with high-energy electron beams," in *Book of Abstracts of XII International Congress of Radiology* (1969), p. 127.

[8]D. W. O. Rogers and A. F. Bielajew, "Differences in electron depth dose curves calculated with EGS and ETRAN and improved energy range relationships," Med. Phys. **13**, 687–694 (1986).

[9]B. B. Sorcini and A. Brahme, "An accurate energy-range relationship for high-energy electron beams in arbitrary materials," Phys. Med. Biol. **39**, 795–811 (1994).

[10]F. M. Khan, K. P. Doppke, K. R. Hogstrom, G. J. Kutcher, R. Nath, S. C. Prasad, J. C. Purdy, M. Rozenfeld, and B. L. Werner, "Clinical electron-beam dosimetry: Report of AAPM Radiation Therapy Committee Task Group 25," Med. Phys. **18**, 73–109 (1991).

[11]M. J. Berger and S. M. Seltzer, "Tables of Energy-Deposition Distributions in Water Phantoms," NBS Report NBSIR 82-2451 (1982).

[12]A. Wu, A. M. Kalend, R. D. Zwicker, and E. S. Sternick, "Comments on the method of energy determination for electron beam in the TG-21 protocol," Med. Phys. **11**, 871–872 (1984).

[13]A. Brahme and H. Svensson, "Specification of electron beam quality from the central-axis depth absorbed-dose distribution," Med. Phys. **3**, 95–102 (1976).

[14]G. X. Ding, D. W. O. Rogers, and T. R. Mackie, "Calculation of stopping-power ratios using realistic clinical electron beams," Med. Phys. **22**, 489–501 (1995).

[15]M. Udale, "Monte Carlo calculations of electron beam parameters for three Philips linear accelerators," Phys. Med. Biol. **37**, 85–105 (1992).

[16]D. W. O. Rogers, B. A. Faddegon, G. X. Ding, C.-M. Ma, J. Wei, and T. R. Mackie, "BEAM: A Monte Carlo code to simulate radiotherapy treatment units," Med. Phys. **22**, 503–524 (1995).

[17]P. Andreo and A. Brahme, "Mean energy in electron beams," Med. Phys. **8**, 682–687 (1981).

[18]B. Grosswendt and M. Roos, "Electron beam absorption in solid and water phantoms: depth scaling and energy-range relations," Phys. Med. Biol. **34**, 509–518 (1989).

[19]W. R. Nelson, H. Hirayama, and D. W. O. Rogers, "The EGS4 code system," Stanford Linear Accelerator Center Report SLAC-265, Stanford, CA (1985).

[20]G. X. Ding and D. W. O. Rogers, "Energy spectra, angular spread, and dose distributions of electron beams from various accelerators used in radiotherapy," National Research Council of Canada Report PIRS-0439 (see http://www.irs.inms.nrc.ca/inms/irs/papers/PIRS439/pirs439.html), April, 1995.

[21]G. X. Ding, D. W. O. Rogers, J. Cygler, and T. R. Mackie, "Electron fluence correction factors used in conversion of dose measured in plastic to dose in water," to be submitted to Med. Phys. (1996).

[22]G. X. Ding, D. W. O. Rogers, J. E. Cygler, J. S. Wei, and T. R. Mackie, "Fluence factors used in conversion of dose measured in plastic to dose in water," Med. Phys. **20**, 1589 (1993).

[23]A. F. Bielajew and D. W. O. Rogers, "PRESTA: The parameter reduced

electron-step transport algorithm for electron Monte Carlo transport," Nucl. Instrum. Methods B **18**, 165–181 (1987).

[24]D. W. O. Rogers and A. F. Bielajew, "Monte Carlo techniques of electron and photon transport for radiation dosimetry," in *The Dosimetry of Ionizing Radiation*, edited by K. R. Kase, B. E. Bjarngard, and F. H. Attix (Academic, New York, 1990), Vol. III, pp. 427–539.

[25]C. Malamut, D. W. O. Rogers, and A. F. Bielajew, "Calculation of water/air stopping-power ratios using EGS4 with explicit treatment of electron—positron differences," Med. Phys. **18**, 1222–1228 (1991).

[26]ICRU, "Stopping powers for electrons and positrons," Report 37, Bethesda, MD, 1984.

[27]S. Duane, A. F. Bielajew, and D. W. O. Rogers, "Use of ICRU-37/NBS collision stopping powers in the EGS4 system," NRCC Report PIRS-0173, Ottawa, March, 1989.

[28]K. A. Johansson, L. O. Mattsson, L. Lindborg, and H. Svensson, "Absorbed-dose determination with ionization chambers in electron and photon beams having energies between 1 and 50 MeV," *IAEA Symposium Proceedings* (IAEA, Vienna, 1977), Paper IAEA-SM-222/35, pp. 243–270.